Journal of Materials Chemistry C

Accepted Manuscript

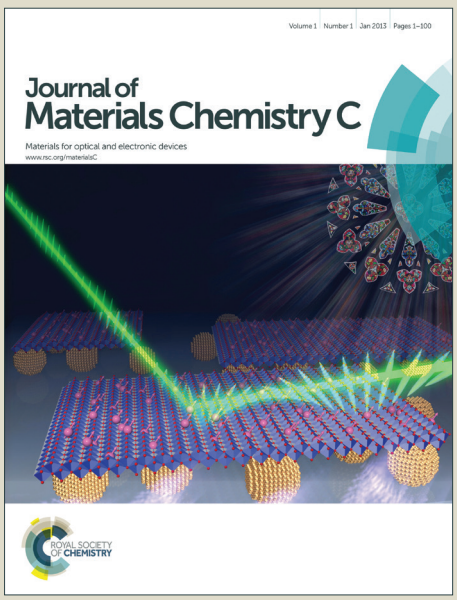

ROYAL SOCIETY OF CHEMISTRY

www.rsc.org/materialsC

Solution Processed and Self-assembled Polymerizable Fullerenes/Metal Oxide as an Interlayer for High Efficient Inverted Polymer Solar Cells

Lin Hu[1], Lie Chen[1,2], Xiaotian Hu[1], Yiwang Chen[*1,2]

[1]Institute of Polymers/College of Chemistry, Nanchang University, 999 Xuefu Avenue, Nanchang 330031, China; [2]Jiangxi Provincial Key Laboratory of New Energy Chemistry, Nanchang University, 999 Xuefu Avenue, Nanchang 330031, China

Abstract: A novel polymerizable fullerene derivative, 2-(2-(2-methoxyethoxy) ethoxy) ethyl undec-10-enyl malonate C_{60} (EEMC), functionalized with ethenyl and tri-(ethylene oxide) (TEO), has been rationally designed and synthesized. The functionalized fullerene can easily self-assemble on surface of ZnO to form an immobilized and robust fullerene/ZnO electron-transporting layer (ETL) for the inverted solar cells. And the solution processed and assembled fullerene/ZnO ETL can be further stabilized by a polymerized network resulting from ethenyl groups undergoing subsequently thermal annealing. The oxygen groups of TEO anchoring on ZnO effectively passivate the surface traps of ZnO and induce a smoother and more hydrophobic surface. Moreover, the polymerized EEMC (PEEMC) also promotes a better matched energy level, more intimate interfacial contact and improves active layer morphology compared to the bare ZnO. As a result, the performance of the inverted solar cell device is improved by incorporation of such novel ETL. Furthermore, methanol treatment on the PEEMC (MT-PEEMC) is found to better optimize the device performance. The device based on a blend of a low band-gap polymer thieno[3,4-b]thiophene/benzodithiophene (PTB7) with [6,6]-phenyl C_{71}-butyric acid methyl ester ($PC_{71}BM$) delivers a high efficiency of 7.5%. Note that a solution-processed solar cell with MT-PEEMC as ETL and a sol-gel derived VO_x as holes transfer layer (HTL) achieves a PCE of 7.3%. In addition, the self-assembled and polymerized interlayer also improves the durability of device lifetime.

Key words: Self-assembly; Fullerenes; Interlayer; Inverted solar cells

[*] Corresponding author. Tel.: +86 791 83969562; fax: +86 791 83969561. *E-mail address*: ywchen@ncu.edu.cn (Y. Chen).

Introduction

Polymeric solar cells (PSCs) have been attracted great attentions in the past decade due to their low-cost, large area, easy solution-based fabrication with mechanical flexibility and the general applicability of organic materials.[1] Recently, the power conversion efficiency (PCE) in excess of 10% has been reported by several groups and constitutes a significant breakthrough in the field of PSCs.[2] Usually there are two main types of device architectures: the conventional and the inverted structure. The PSCs with conventional structure always suffer from the rapidly reduced stability and performance of the devices due to the easily oxidized low work function metal and etching of ITO by the acidic poly (3, 4-ethylene dioxythiophene): poly (styrene sulfonic acid) (PEDOT: PSS) hole-transporting layer (HTL).[3] To ameliorate these problems, an inverted device structure is fabricated by reversing the polarity of charge collection in a conventional structure.[4] In this architecture, a high work function metal (Ag) is used as anode, while an n-type metal oxide (ZnO or TiO_x) is coated onto ITO as cathode, as a result the device stability has been found to be improved greatly.[5]

However, most inverted PSCs, especially based on poly (3-hexylthiophene) (P3HT): (6, 6)-phenyl-C_{61} butyric acid methyl ester ($PC_{61}BM$), show inferior performance to the conventional ones due to unfavorable morphology of active layer and incompatible chemical interfaces.[6] Moreover, surface hydroxyl groups on metal oxide are known to act as charge traps, which will restrict the mobility of the unbound electrons and facilitate the carries to recombine, ultimately resulting in an inferior current.[7] In order to further improve the performance of the inverted PSCs, an additional n-type fullerene derivative as electron transport layer (ETL) is commonly incorporated between the inorganic metal oxide and the organic active layer to modulation of the energy levels and interfacial contact.[8] Previously, a variety of fullerene-based self-assembled monolayers (SAMs) bearing hydroxyl, carboxylic acid or tri-(ethylene oxide) (TEO), have been developed and worked well in improving the device performance.[8a,9] With these anchoring groups interacting with the hydroxyl on the metal oxide, subsequently it can form an immobilized SAM, which can passivate

the electron traps and suppress the carriers to recombine effectively.[10] However, the SAM formation insufficiently fully filled and covered the surface of metal oxides at the molecular scale, and it can be easy desorption of the molecules during wet processing, leading to localized defects in this interlayer.[11]

An effective strategy to overcome the deficiency of SAM is to introduce a cross-linkable or polymerizable fullerene derivative to produce a robust and solvent resistant thin film on ZnO surface.[12] The interlayer of fullerene derivative allows a subsequent active layer to be successfully deposited on top of this SAM without causing interfacial erosion and achieves an inverted device by all-solution processing. These fullerene derivatives can also form a firm interlayer through polymerization or cross-linking reaction which can avoid a direct contact between the ZnO and active layer. Hsu group reported an inverted solar cell device based on a cross-linkable PCBSD as an interlayer obtaining an improved PCE of 4.4% in comparison to a reference device (PCE = 3.5%) without this interlayer.[13]

Combination of the advantages of the polymerization approaches with the self-assembly property, a novel solution processed fullerene derivative attached with TEO group and polymerizable ethenyl group has been developed as an ETL for PSCs. The design and synthesis routes of 2-(2-(2-methoxyethoxy) ethoxy) ethyl undec-10-enyl malonate C_{60} (EEMC) was shown in **Scheme 1**. Due to the strong hydrogen bond interaction between EEMC and the metal oxide, the functionalized fullerene can easily self-assemble on surface of ZnO and passivate the surface defects of ZnO. More importantly, ethenyl groups undergoing subsequently thermal annealing can generate polymerized EEMC (PEEMC) with a dense network to further stabilize the assembled fullerene/ZnO ETL. With this PEEMC/ZnO interlayer applied in an inverted architecture, it promotes a matched energy level, intimate interfacial contact and well-defined active layer morphology. Besides, methanol treatment on the assembled fullerene/ZnO before polymerization is more favorable. As a result, incorporation of this self-assembled and polymerized fullerene/ZnO into the inverted

solar cells based on P3HT:$PC_{61}BM$ as an interlayer have achieved a PCE of 3.8% with 36% enhancement and remarkable long-term stability in air in comparison to the control device without this interlayer. The novel interlayer also shows good universality in the device based on a blend of a low band-gap polymer PTB7 with $PC_{71}BM$, which delivers a high efficiency of 7.5% with good stability. This noteworthy efficiency can be well maintained in a solution processed device with sol-gel derived VO_x to replace the evaporated MoO_3 as holes transfer layer, which is beneficial for large-scale and high-throughput production of polymer solar cell.

Results and Discussion

The synthesis of the EEMC is shown in **Scheme 2**. The malonyl chloride **1** was added dropwise to the mixed solution of 10-undecen-1-ol **2** and triethylene glycol monomethyl ether **3** and reacted with them simultaneously to afford compound **4**. Under basic condition, the Bingel reaction of compound **4** with C_{60} in the presence of iodine was carried out to obtain the compound EEMC. The synthetic details and the ^1H NMR spectra of compound **4** and EEMC are shown in **Figure S1** (**Supporting Information**). The EEMC is thermal and air stable, and soluble in common solvents such as chloroform, chlorobenzene, and toluene.

In this report, ZnO is used to act as the hole-blocking and electron-selective layer in the inverted solar cells due to its high electron mobility and suitable energy levels. The ZnO nanoparticles with a thickness of 30 nm were firstly prepared on the ITO substrate according to the literature.[5a] Self-assembled and polymerizable electron transport layer PEEMC with a thickness of 12 nm was prepared from a solution of EEMC spun-cast on top of the surface of ZnO and then polymerized at 150 °C for half an hour. Inspired by the recent work on polar solvent treatment to improve the device performance,[14] a methanol treated (MT) polymerized film (MT-PEEMC) was adopted by spin coating pure methanol on film surface before thermal polymerization (**details in the supporting information**). The thermal polymerization of the PEEMC film is confirmed by the almost unchanged UV-Vis absorption spectra of the samples

before and after rinsing with *o*-dichlorobenzene **(Figure 1)**. Notably, UV-Vis absorption bands of the unpolymerized EEMC almost disappeared after rinsing with o-dichlorobenzene. Thus robust and dense polymerized network with considerable organic solvent resistance can ensure the PEEMC layer not washed away during the deposition of the active layer. Surface contact angel measurement was used to monitor the surface alteration **(Figure S2, Supporting Information)**. As seen from the images, the bare ZnO surface exhibits a contact angel of ca.49°. After an ultra thin layer of polymerized PEEMC spin-coated on the ZnO interface, the wetting angel to deionized water of ZnO/PEEMC increases to ca.78°. The increased wetting angel indicates that the hydrophilic ZnO surface modified by the PEEMC can generate a more hydrophobic surface, which would potentially facilitate the deposition of the active layer. When the EEMC film treated with methanol before thermal polymerization, the contact angel of the MT-PEEMC slightly increases to 82°, probably owing to the denser film developed by methanol treatment, which will reduce the defects and traps in the ETL for more efficient charge extraction and collection. The contact angel of PEEMC is still smaller than that of C_{60} (**Figure S2**), again confirming the successful modification on the fullerene by TEO.

To investigate the molecular interactions between the fullerene-based layer and the ZnO, the surfaces were characterized by X-ray photoelectron spectroscopy (XPS). **Figure 2(a)** shows the survey XPS spectra of novel ETLs. Bare ZnO, ZnO/PEEMC and ZnO/MT-PEEMC all exhibit Zn 2p peaks and O 1s. Through the high-resolution XPS spectra **(Figure 2 (b))**, it is obvious that the pristine ZnO surface exhibits a Zn $2p_{1/2}$ peak centered at 1044.7 eV and a Zn $2p_{3/2}$ centered at 1021.5 eV, whereas the two peaks in spectrum of ZnO/PEEMC display at 1044.2 eV and 1021.1 eV, respectively. The shift to the lower binding energy of ZnO/PEEMC is ascribed to the higher negative charge density on Zn. Similarly, as to the high-resolution XPS spectra of O 1s, the peak corresponding to O atoms in a ZnO nanoparticle also moves to the higher binding energy. It indicates the reduced negative charge density O, which was ascribed to the hydrogen bond interaction between the fullerene and ZnO.[5a,15] The

shifts in peaks of the Zn 2p and O 1s give an evidence that the PEEMC has successfully assembled on the surface of ZnO via the strong molecular interactions between –OH of ZnO nanoparticles and -O- in the terminal TEO of PEEMC, which is beneficial for reducing the traps and defects by filling the voids with the C-EEMC on the uneven ZnO surface. Moreover, after methanol treatment, the peaks of the Zn 2p and O 1s further shift to the lower and higher binding energy, respectively, suggesting that the polar solvent treatment can make the TEO functionality of PEEMC more intimate with the ZnO surface. To further investigate whether the EEMC can passivate and surface traps and defects of ZnO, the photoluminescence (PL) measurement of ZnO modified by EEMC with different concentration were carried out, as demonstrated in **Figure S3** (**Supporting Information**). Compared with the pristine ZnO with a strong defect emission at 400~550nm, the EEMC modified ZnO exhibit a considerably restrained defect emission indicative of the effectively passivated surface of ZnO. The reduced surface traps on ZnO can suppress the trap-assisted interfacial charge recombination and promote the charge transport in the PSC.[16]

It's believed that an electron transport layer with proper LUMO level can presumably yield a better energy-level alignment and ohmic contact at the cathode/PCBM interface to promote the electronic extraction and transportation. However, the LUMO level of the bare ZnO ETL does not well match with the LUMO of PCBM. Therefore, ultraviolet photoelectron spectroscopy (UPS) was performed study the shifting of the surface energy levels of the PEEMC and MT-PEEMC on the top of ITO/ZnO. As shown in **Figure 3(a)**, the high binding energy cutoff from a spectrum is E_{cutoff}, which is estimated by linear extrapolation to zero at the yield of secondary electrons.[17] E_{onset} is the HOMO energy onset, referred to as the binding energy onset, which is shown in **Figure 3(b)**. From **Table 1**, the E_{cutoff} of ZnO, ZnO/PEEMC and ZnO/MT-PEEMC are 14.25, 14.32 and 14.40 eV, respectively, and the corresponding E_{onset} are 0.81, 0.77 and 0.70 eV. As the incident photon energy hν is 21.22 eV, the HOMO energies are determined according to the followed equation:[18]

$$-E_{HOMO} = h\nu - (E_{cutoff} - E_{onset})$$

Consequently, the calculated HOMO energies for ZnO, ZnO/PEEMC and ZnO/MT-PEEMC are -7.78, -7.67, -7.52 eV, respectively. In light of these HOMO energies and the optical gaps (3.38 eV) obtained from the UV-vis absorption spectra, the estimated LUMO energy levels are -4.50 eV for bare ZnO, -4.39 eV for ZnO/ PEEMC and -4.25 eV for ZnO/MT-PEEMC, respectively. An Energy-level diagram is constructed to illustrate the shift of the energy levels distinctly in **Figure 3(c)**. The shifts in LUMO energies levels indicate that the LUMO energy levels of ZnO are fine-tuned by coating a thin layer of functionalized fullerenes. With respect to the ZnO/PEEMC, the ZnO/MT-PEEMC seems to promote a better energy alignment for electronic extraction and collection, due to the stronger interaction between the ZnO and MT-PEEMC induced by the methanol treatment. In **Figure 3(d)**, the P3HT absorbed the light to emit photoluminescence (PL) intensity around 640 nm. When P3HT was blended with the EEMC, the PL intensity was substantially quenched as the increase of the EEMC concentration. Such PL quenching is indicative of the efficient charge transfer between EEMC and P3HT. As a result, the suitable LUMO level also enables fullerene-based interlayer to act as an acceptor to provide extra exciton separation center for charger carrier generation[19].

The surface morphology of the self-assembled and polymerized interlayer on ITO/ZnO was also investigated by scanning electron microscopy (SEM). **Figure 4** compares the images acquired from SEM on ZnO/PEEMC and ZnO/MT-PEEMC with bare ZnO. The SEM image shows that bare ZnO surface is relatively smooth and dense (**Figure 4a**), implying uniformly covered ZnO nanoparticles on the ITO substrate. When the ZnO surface is modified with PEEMC, the morphology of ETLs has been greatly changed. The PEEMC tends to self-assemble into wormlike wrinkles on the ZnO surface because of intermolecular interactions between TEO functionality of EEMC and ZnO, as revealed by **Figure 4b**. As expected, these wormlike wrinkles become more obvious and homogeneous in the image of MT-PEEMC film undergoing methanol treatment (**Figure 4c)**. These wormlike wrinkles with micrometer-scale fiber could favor an imitate contact and enlarge the interfacial area

between the ETL and active layer for charge extraction and transportation. Since fullerene-based interlayer can also act as an extra acceptor for charge separation, the assembled wormlike wrinkles may provide a desirable electron transport pathway for electron transport to the cathode.

As mentioned above, the self-assembled and polymerized fullerene interlayer causes a great change on the interface morphology and substantially alters the wettability of ZnO. the atomic force microscopy (AFM) images were thus examined to elucidate the effect of the PEEMC interlayer on the morphology of the upper active layer. **Figure 5** shows AFM tapping mode topography images of P3HT:$PC_{61}BM$ films on top of ITO/ZnO, ITO/ZnO/PEEMC and ITO/ZnO/MT-PEEMC. All samples were prepared following the same condition as that conducted for device fabrication, without deposition of the MoO_3 layer and the top metal electrode. From these AFM images, we can observe that the P3HT:$PC_{61}BM$ film deposited on ITO/ZnO show a coarse surface roughness of 2.4 nm with larger red and green areas reflecting extended phase separation. This pronounced phase separation between donor and acceptor domains will result in unfavorable conditions for charge separation and transport, as well as poor contact between the active layer and the electrode. However, after incorporation of the polymerized EEMC between the ZnO/active layer interface, the AFM images of P3HT:$PC_{61}BM$ film display obvious variation in contrast and reflect a rather uniform and smooth morphology with reduced surface roughness (1.5 nm). Moreover, the methanol treatment further promotes a better developed morphology of P3HT:$PC_{61}BM$ active layer. In **Figure 5**, the AFM image of active layer deposition on ITO/ZnO/MT-PEEMC shows homogenous and well-dispersed nanostructure with surface roughness of 1.2 nm. It should be noted that compared with the P3HT:$PC_{61}BM$ casting on the ZnO/PEEMC without methanol treatment, the one deposition on MT-PEEMC reveals a larger number of nano-scale interconnected domains. A smoother surface resulting a intimated contact with the upper layer, which is very desirable for high performance OPV, thus an improved J_{sc} and FF from the inverted structure with these fullerene modified ETLs are anticipated.

To verify the superiority of this self-assembled and polymerized fullerene modified ZnO as ETL in PSCs, a multilayer inverted device structure was fabricated with a configuration of ITO/ZnO/SAM/P3HT:$PC_{61}BM$ (1:1, w/w)/e-MoO_3/Ag. After deposition a layer of the functionalized fullerene on ZnO, thermal annealing at 150^oC is performed in order to generate the polymerized network of the PEEMC. A thin layer evaporated MoO_3 (e-MoO_3) is used here as holes transport layer (HTL). Under the same condition **(Details in the Supporting information)**, a series of different concentration ratios of EEMC as ETL were tested to find an optima for the device fabrication. The illuminated current-voltage (*J-V*) curves of these devices based on different concentration ratios of EEMC are shown in **Figure S4** and **Figure 6**, and the corresponding device parameters are summarized in **Table S1** and **Table 2**. From this table we can see that, the control device (ITO/ZnO/P3HT:$PC_{61}BM$ (1:1, w/w)/e-MoO_3/Ag, defined as **Device A**) shows a PCE of 2.7%, with a short-circuit current (J_{sc}) of 8.59 mA/cm^2, an open-circuit voltage (V_{oc}) of 0.60 V and a fill factor (FF) of 51.7%. The devices performance was relative with the concentration ratios of EEMC. It is found that when the concentration of the EEMC is 4 mg/ml, the device based on the inverted structure (ITO/ZnO/PEEMC/P3HT:$PC_{61}BM$ (1:1, w/w)/e-MoO_3/Ag, defined as **Device B**) with ZnO/PEEMC ETL performs best and shows 29% improvement of PCE over the control one. The improved PCE should be ascribed to the allover enhanced device parameters, especially J_{sc} and FF. The slightly improved V_{oc} is related to the better energy alignment caused by incorporation of the PEEMC, in good agreement with the UPS observation. The enhancement in J_{sc} and FF is owing to the effective charge carrier extraction, transportation and collection. It probably results from the favorable morphology of active layer, improved interfacial wettability and efficient holes block caused by the novel ETL.

Further optimization on the device is introduction of a polar solvent methanol to infiltrate the EEMC before thermal polymerization. Delightfully, the PCE is enhanced from 3.5% for **Device B** to 3.8% for **Device C**

(ITO/ZnO/MT-PEEMC/P3HT:$PC_{61}BM$ (1:1, w/w)/e-MoO_3/Ag), revealing a 35.7% improvement in comparison to the control one. The better matched energy level, less ZnO defects, more intimate interfacial contact and improved active layer morphology induced by MT-PEEMC should be responsible for the improved device performance. The enhanced current and PCE of the devices are well consistent with the external quantum efficiency (EQE) spectra of the devices, as shown in **Figure 6**. The difference between tested and EQE calculated J_{SC} value is within the experimental error.

Successful application of the PEEMC interlayer in P3HT:$PC_{61}BM$-based inverted solar cell inspired us to employ it into other type device to investigate its universal validity. A narrow band gap polymer PTB7 blended with $PC_{71}BM$ was incorporated as the active layer in an inverted device. The *J-V* curves and the characteristics of the device with and without MT-PEEMC interlayer as electron transport layer are shown in **Figure 7 and Table 2**. The control device (**Device D**) only with bare ZnO ETL gives a V_{oc} of 0.71 V, a J_{sc} of 16.60 mA/cm^2, a FF of 56.0%, and a PCE of 6.6%, whereas the **Device E** with ZnO/MT-PEEMC interlayer delivers a V_{oc} of 0.72 V, a J_{sc} of 17.56 mA/cm^2, a FF of 58.5%, and a PCE of 7.5%, which represents a 13.6% enhancement in PCE. Similarly, the improvement in the PCE results from the overall improved V_{oc}, J_{sc} and FF. To meet with large-scale and high-throughput production of polymer solar cell, a sol-gel derived VO_x (s-VO_x) is introduced to replace the evaporated MoO_3 (e-MoO_3) as holes transfer layer to fabricate **Device F**. Intriguingly, the **Device F** with solution processed VO_x HTL (ITO/ZnO/MT-PEEMC/PTB7:$PC_{71}BM$ (1:1.5, w/w)/s-VO_x/Ag) shows a comparable efficiency of 7.3% to the device with evaporated MoO_3 (**Figure 7 and Table 2**).[20] It should be noted that this efficiency is obtained from the all solution processed device except for the electrode. The corresponding EQE spectra of the devices are also shown in **Figure S4**. Thus it can be seen that this self-assembled and polymerized interlayer shows a great potential for solution processed OPVs.

To investigate the effect of polymerized interlayer on the device stability, the air-stability of the unencapsulated inverted devices with or without the polymerized EEMC interlayer were periodically measured for 30 days (humidity, ~55%; ~25 ℃) without any encapsulation barrier **(Figure 8)**. Due to the oxygen and moisture at the surface of ZnO may reduce the electron extracted, the **Device A** and **D** without functionalized fullerene interlayer retain only 30% and 24% of their original PCE after being exposed to ambient conditions **(Figure 8a)**. However, the devices with polymerized EEMC modified ZnO exhibit much better long-term stability, especially for the one with MT-PEEMC interlayer, retaining about 70% of the initial efficiency for **Device C** and 65% for **Device E**, together with well-maintained V_{oc}, J_{sc} and FF **(Figure 8b, c** and **d)**. Therefore, the polymerized network and strong hydrogen bond interaction can stabilize the interfacial layer to achieve an oxygen-resistant ZnO, leading to the improved stability of the devices. Further, the denser polymerized network and more imitate interfacial contact induced by methanol treatment might passivate the hot spots generated in the ZnO to suppress the leakage current, and prevent the gradual mutual penetration between the ZnO and the active layer as the operational time increases, consequently enhancing the durability of device lifetime.

Conclusions

In conclusion, we have successfully designed and synthesized a novel C_{60}-based n-type material EEMC, functionalized with tri(ethylene oxide) (TEO) and polymerizable ethenyl groups, as self-assembled and polymerized electron transport layer (ETL) to fabricate high-performance and long-term stable inverted solar cells. The EEMC is capable of self-assembly on the ZnO surface to form an adhesive monolayer with intimate contact and subsequently undergoing polymerization to produce a robust thin film with good solvent resistant. This interlayer not only passivates the electron-traps and modulates the energy-level alignment at the PCBM-ZnO interface effectively, but also contributes to a desirable nanostructure of the active layer. And the methanol treatment on the polymerized EEMC can boost these advantages of this novel interlayer. An inverted solar cell device based on

P3HT:$PC_{61}BM$ with MT-PEEMC exhibits a 35.7% improvement of PCE in comparison to the control device. A further improved PCE of 7.5% has been achieved in the device based on PTB7:$PC_{71}BM$ as active layer. This noteworthy efficiency can be well maintained in a solution processed device with sol-gel derived VO_x to replace the evaporated MoO_3 as holes transfer layer. In addition, incorporation of this polymerized fullerene interlayer endows the devices with improved air stability in ambient conditions. Therefore, integration of the advantages of self-assembly and polymerization in a single fullerene-based material, provides a simple and promising method for all solution-processed, air-stable and high-performance polymer solar cells.

ACKNOWLEDGEMENTS

This work was supported by the National Natural Science Foundation of China (51273088, 51263016 and 51473075) and Doctoral Programs Foundation of Ministry of Education of China (Grants 20133601110004).

Reference:

1 (a) B. C. Thompson and J. M. Frechet, *Angew. Chem., Int. Ed.,* 2008, **47**, 58; (b) S. H. Park, A. Roy, S. Beaupré, S. Cho, N. Coates, J. S. Moon, D. Moses, M. Leclerc, K. Lee and A. J. Heeger, *Nat. Photonics*, 2009, **3**, 297; (c) J. H. Seo, A. Gutacker, Y. Sun, H. Wu, F. Huang, Y. Cao, U. Scherf, A. J. Heeger and G. C. Bazan, *J. Am. Chem. Soc.*, 2011, **133**, 8416; (d) Z. He, C. Zhong, S. Su, M. Xu, H. Wu and Y. Cao, *Nat. Photonics*, 2012, **6**, 591.

2 (a) J. You, C. C. Chen, Z. Hong, K. Yoshimura, K. Ohya, R. Xu, S. Ye, J. Gao, G. Li and Y. Yang, *Adv. Mater.*, 2013, **25**, 3973; (b)J. You, L. Dou, K. Yoshimura, T. Kato, K. Ohya, T. Moriarty, K. Emery, C. C. Chen, J. Gao, G. Li and Y. Yang, *Nat. Commun.*, 2013, **4**, 1446.

3 (a) M. P. de Jong, L. J. van Ijzendoorn and M. J. A. de Voigt, *Appl. Phys. Lett*., 2000, **77**, 2255; (b) S. K. Hau, H.-L. Yip, N. S. Baek, J. Zou, K. O'Malley and A. K. Y. Jen, *Appl. Phys. Lett*., 2008, **92**, 253301.

4 (a) H.-H. Liao, L.-M. Chen, Z. Xu, G. Li and Y. Yang, *Appl. Phys. Lett.,* 2008, **92**, 173303; (b) C. S. Kao, F. C. Chen, C. W. Liao, M. H. Huang and C.-S. Hsu. *Appl. Phys. Lett.,* 2012, **101**, 193902.

5 (a) Y. Sun, J. H. Seo, C. J. Takacs, J. Seifter and A. J. Heeger, *Adv. Mater.*, 2011, **23**, 1679-1683; (b) H.-C. Liao, C.-H. Lee, Y.-C. Ho, M.-H. Jao, C.-M. Tsai, C.-M. Chuang, J.-J. Shyue, Y.-F. Chen and W.-F. Su, *J. Mater. Chem.*, 2012, **22**, 10589. (c) F. C. Chen, J. L. Wu and Y. Hung, *Appl. Phys. Lett.,* 2010, **96**, 193304.

6 (a) M. S. White, D. C. Olson, S. E. Shaheen, N. Kopidakis and D. S. Ginley, *Appl. Phys. Lett.,* 2006, **89**, 143517; (b) G. K. Mor, K. Shankar, M. Paulose, O. K. Varghese and C. A. Grimes, *Appl. Phys. Lett.,* 2007, **91**, 152111; (c) Z. Liang, Q. Zhang, O. Wiranwetchayan, J. Xi, Z. Yang, K. Park, C. Li and G. Cao, *Adv. Funct. Mater*., 2012, **22**, 2194; (d) C. Waldauf, M. Morana, P. Denk, P. Schilinsky, K. Coakley, S. A. Choulis and C. J. Brabec, *Appl. Phys. Lett.,* 2006, **89**, 233517.

7 (a) M. Einat and N. Einat, *Appl. Phys. Lett.,* 2006, **89**, 073505; (b) S. Lee, B. Koo, J. Shin, E. Lee, H. Park and H. Kim, *Appl. Phys. Lett.,* 2006, **88**, 162109; (c) D. F. Figer, *Nature,* 2005, **434**, 192.

8 (a) C.-Z. Li, H.-L. Yip and A. K. Y. Jen, *J. Mater. Chem.,* 2012, **22**, 4161; (b) H. Ma, H.-L. Yip, F. Huang and A. K. Y. Jen, *Adv.Funct. Mater*., 2010, **20**, 1371.

9 (a) J. W. Jung, J. W. Jo and W. H. Jo, *Adv. Mater.*, 2011, **23**, 1782; (b) S. Chen, X. Du, G. Ye, J. Cao, H. Sun, Z. Xiao and L. Ding, *J. Mater. Chem. A*, 2013, **1**, 11170.

10 (a) S. K. Hau, H.-L. Yip, H. Ma and A. K. Y. Jen, *Appl. Phys. Lett.,* 2008, **93**, 233304; (b) C. Duan, C. Zhong, C. Liu, F. Huang and Y. Cao, *Chem. Mater.*, 2012, **24**, 1682.

11 S. K. Hau, Y.-J. Cheng, H.-L. Yip, Y. Zhang, H. Ma and A. K. Y. Jen, *ACS Appl. Mater. Interfaces.*, 2010, **2**, 1892.

12 (a) Y.-J. Cheng, C.-H. Hsieh, Y. He, C.-S. Hsu and Y. Li, *J. Am. Chem. Soc.*, 2010, **132**, 17381; (b) Y.-J. Cheng, C.-H. Hsieh, P.-J. Li and C.-S. Hsu, *Adv.Funct. Mater*., 2011, **21**, 1723; (c) Y.-J. Cheng, F.-Y. Cao, W.-C. Lin, C.-H. Chen and C.-H. Hsieh, *Chem. Mater.*, 2011, **23**, 1512; (d) W.-W. Liang, C.-Y. Chang, Y.-Y. Lai, S.-W. Cheng, H.-H. Chang, Y.-Y. Lai, Y.-J. Cheng, C.-L. Wang and C.-S. Hsu, *Macromolecules*, 2013, **46**, 4781.

13 C.-H. Hsieh, Y.-J. Cheng, P.-J. Li, C.-H. Chen, M. Dubosc, R.-M. Liang and C.-S. Hsu, *J. Am. Chem. Soc.*, 2010, **132**, 4887.

14 (a) K. Zhang, Z. Hu, C. Duan, L. Ying, F. Huang and Y. Cao, *Nanotechnology*, 2013, **24**, 484003; (b) B. R. Lee, E. D. Jung, Y. S. Nam, M. Jung, J. S. Park, S. Lee, H. Choi, S. J. Ko, N. R. Shin, Y. K. Kim, S. O. Kim, J. Y. Kim, H. J. Shin, S. Cho and M. H. Song, *Adv. Mater.*, 2014, **26**, 494.

15 C. E. Small, S. Chen, J. Subbiah, C. M. Amb, S.-W. Tsang, T.-H. Lai, J. R. Reynolds and F. So, *Nat.*

Photonics, 2012, **6**, 115.

16 (a) T. Hu, F. Li, K. Yuan and Y. Chen, *ACS Appl. Mater. Interfaces.*, 2013, **5**, 5763; (b) S. Shao, K. Zheng, T. Pullerits and F. Zhang, *ACS Appl. Mater. Interfaces.*, 2013, **5**, 380.

17 (a) I. Hill and A. Kahn, *J.Appl.Phys*. 1998, **84**, 5583-5586; (b) C. Tengstedt, W. Osikowicz, W. R. Salaneck, I. D. Parker, C.-H. Hsu and M. Fahlman, *Appl. Phys. Lett.,* 2006, **88**, 053502.

18 S. Braun, W. R. Salaneck and M. Fahlman, *Adv. Mater.*, 2009, **21**, 1450.

19 (a) K. Yuan, L. Chen, L. Tan, Y. Chen, *Chem. Eur. J.,* 2014, **20**, 6010. (b) J. D. Douglas, M. S. Chen, J. R. Niskala, O. P. Lee, A. T. Yiu, E. P. Young and J. M. J. Fréchet, *Adv. Mater*., 2014, **26**, 4313

20 Y.-H. Chao, J.-S. Wu, C.-E. Wu, J.-F. Jheng, C.-L. Wang and C.-S. Hsu, *Adv. Energy Mater.*, 2013, **3**, 1279.

Scheme 1. The schematic diagram of the EEMC interlayer applied in an inverted device.

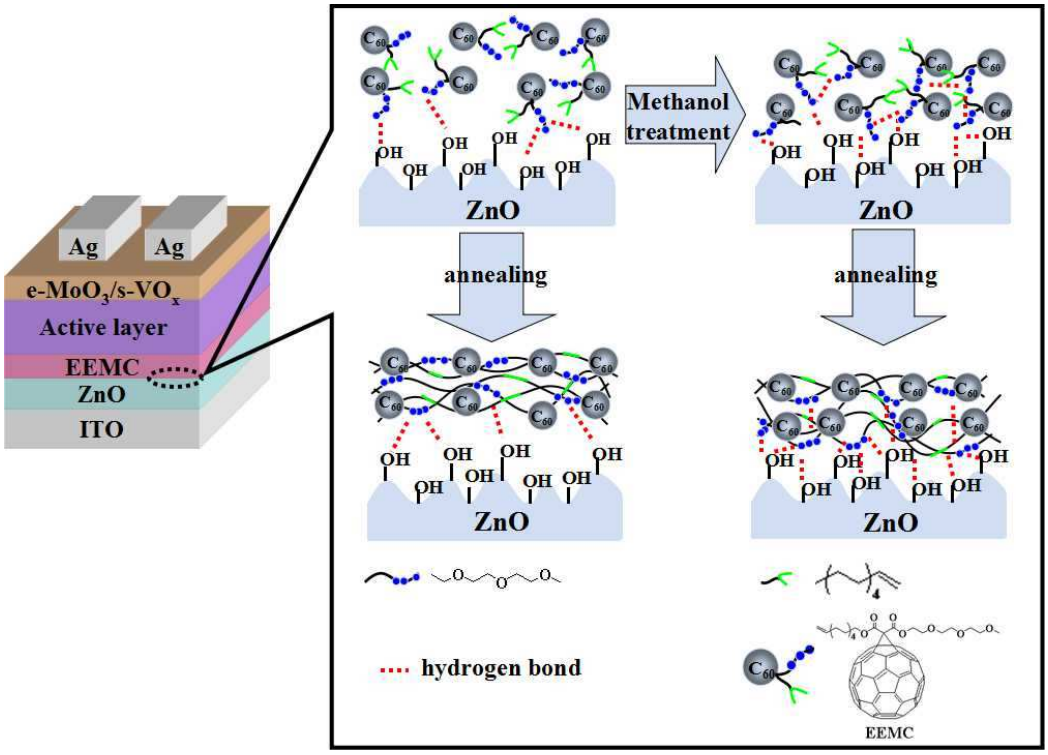

Scheme 2. The synthetic routes of the EEMC.

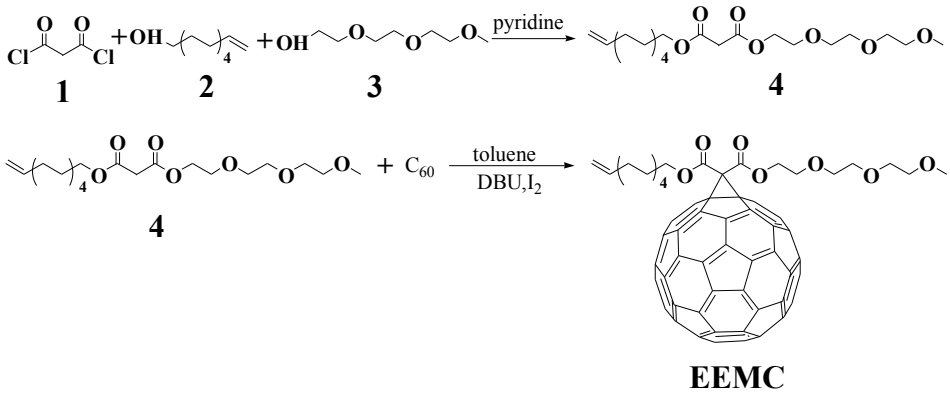

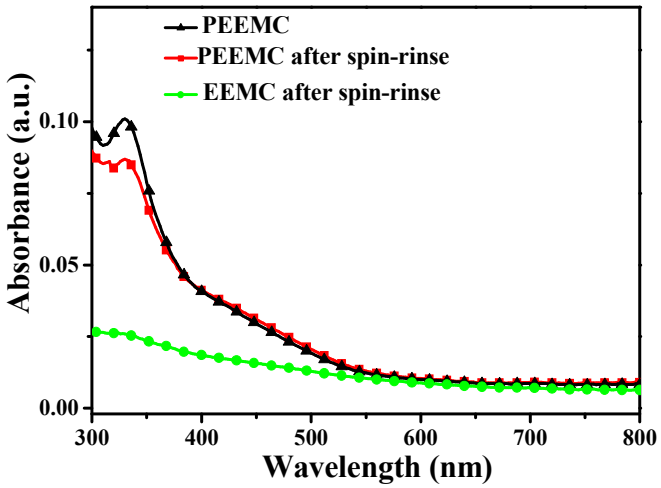

Figure 1. Absorption spectra of the polymerized EEMC before (triangles) and after (squares) rinsing with dichlorobenzene and unpolymerized EEMC (circle) layer after rinsing with o-dichlorobenzene.

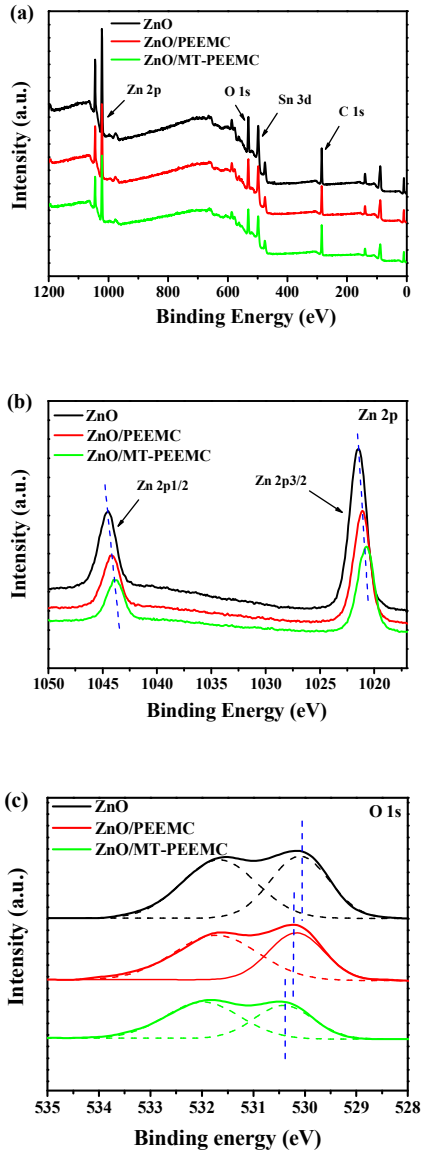

Figure 2. (a) Survey X-ray photoelectron spectra and high-resolution XPS of **(b)** Zn 2p, **(c)** O 1s on the surface of ZnO; ZnO/PEEMC; ZnO/PEEMC with methanol treatment on ITO substrate.

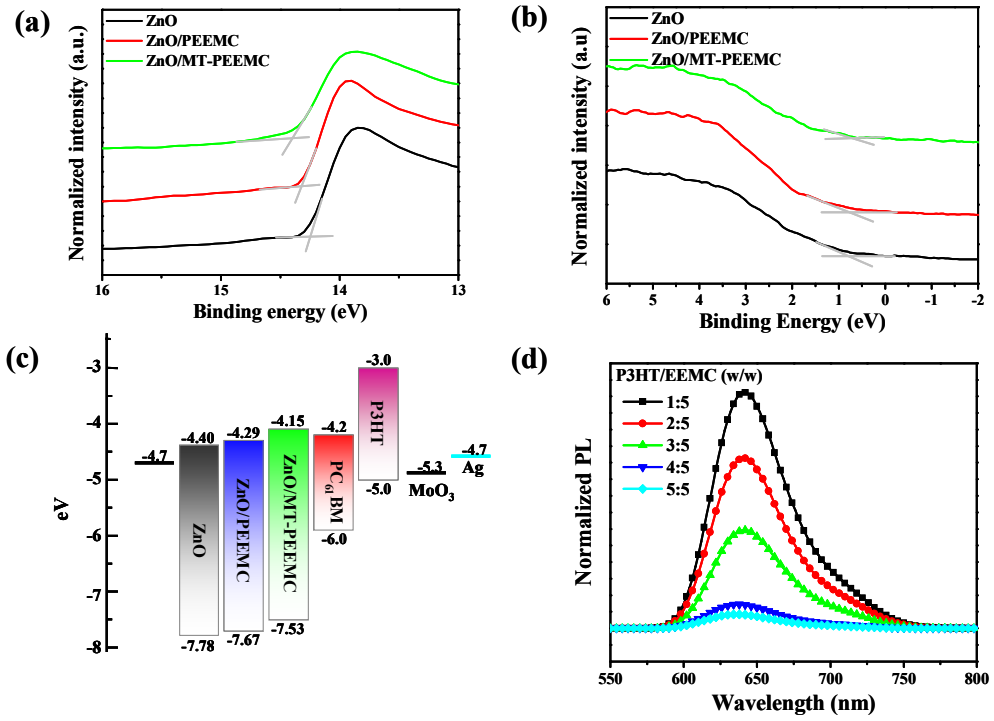

Figure 3. (a) Ultraviolet photoelectron spectroscopy (UPS) spectra of the inelastic cutoff region; **(b)** the HOMO region of ZnO; ZnO/PEEMC; ZnO/MT-PEEMC as ETLs; **(c)** Energy-level diagram of the inverted structures and electrical contacts of the ETLs with the LUMO level of $PC_{61}BM$; **(d)** the photoluminescence (PL) spectra of P3HT blended with EEMC of different concentration.

Table 1. Energy levels of the ETLs

ETL	E_{cutoff} (eV)	E_{onset} (eV)	HOMO (eV)	LUMO (eV)
ZnO	14.25	0.81	-7.78	-4.40
ZnO/PEEMC	14.32	0.77	-7.67	-4.29
ZnO/MT-PEEMC	14.40	0.70	-7.53	-4.15

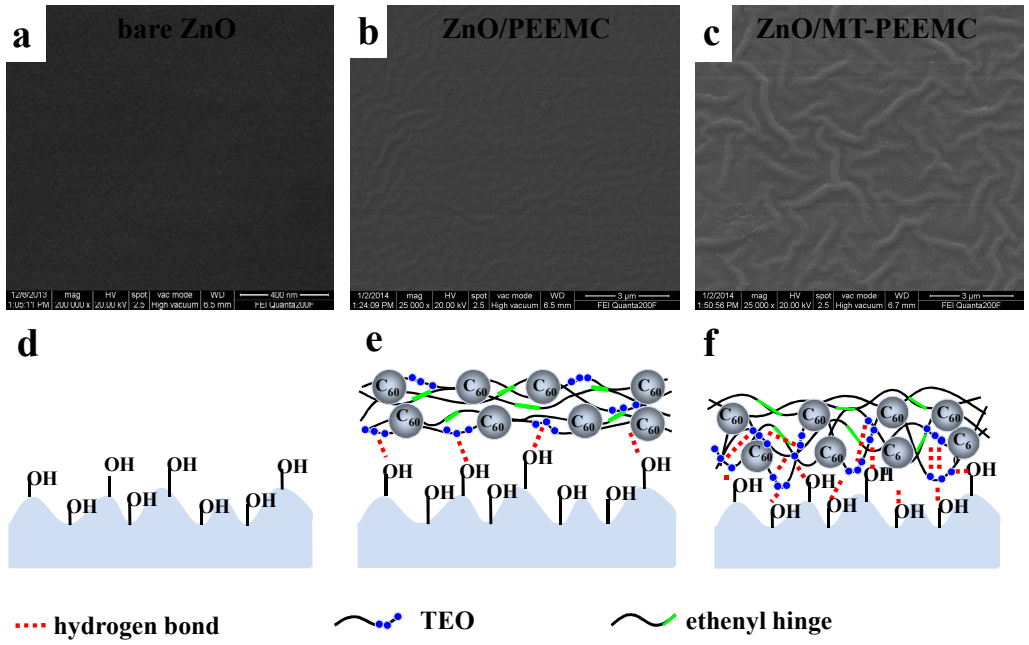

Figure 4. SEM images of surfaces **(a)** bare ZnO, **(b)** ZnO/PEEMC magnification of 25000×, **(c)** ZnO/MT-PEEMC magnification of 25000× and the corresponding sketch map **(d)**, **(e)**, **(f)**, respectively.

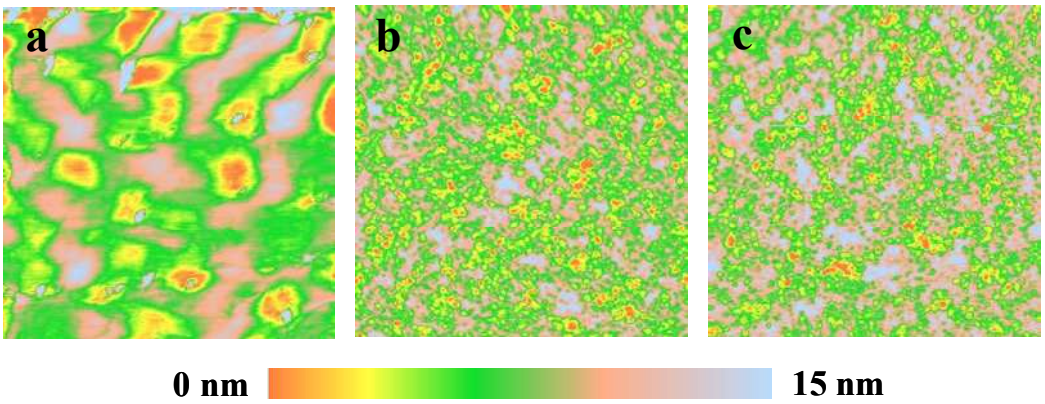

Figure 5. The AFM morphology images (3μm×3μm) of **(a)** ZnO/P3HT:$PC_{61}BM$, **(b)** ZnO/PEEMC/P3HT:$PC_{61}BM$, **(c)** ZnO/MT-PEEMC/P3HT:$PC_{61}BM$.

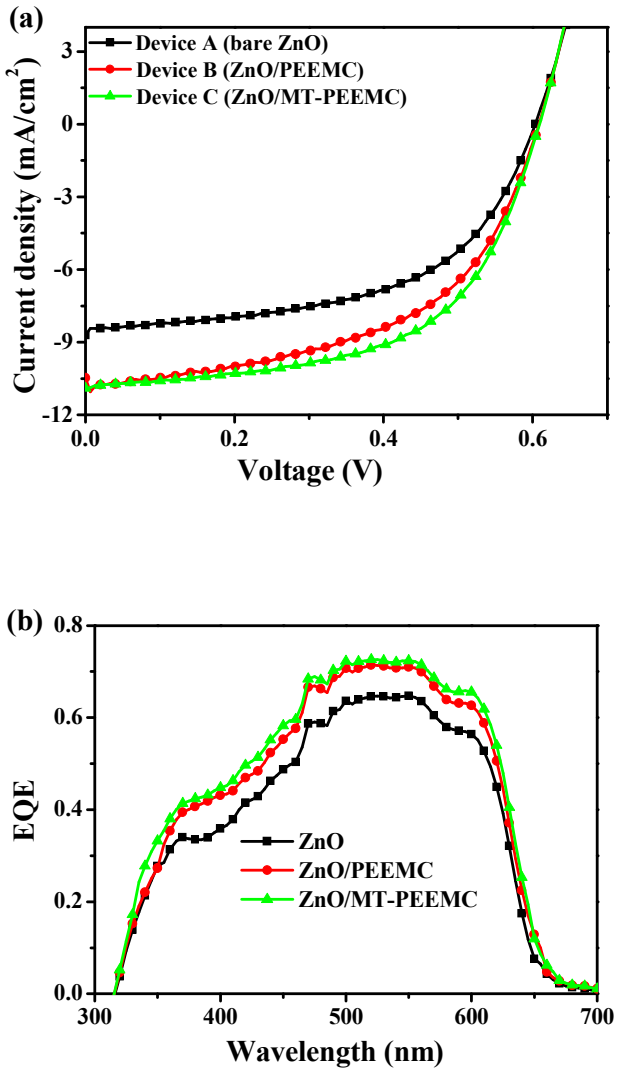

Figure 6. (a) *J-V* curves of device A, B, and C under AM 1.5G illumination at 100 mW/cm^2. **(b)** Corresponding EQE spectra of devices A, B, and C.

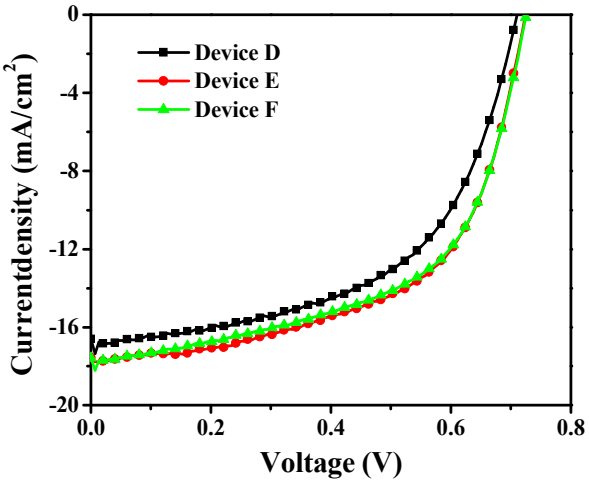

Figure 7. *J–V* characteristics of the I-PSCs: Device D, ITO/ZnO/PTB7:$PC_{71}BM$ (1:1.5, w/w)/e-MoO_3/Ag; Device E, ITO/ZnO/MT-PEEMC/PTB7:$PC_{71}BM$ (1:1.5, w/w)/e-MoO_3/Ag; Device F, ITO/ZnO/MT-PEEMC/PTB7:$PC_{71}BM$ (1:1.5, w/w)/ s-VO_x/Ag.

Table 2. Performance parameters of devices A, B, C with P3HT:$PC_{61}BM$ as active layer and devices D, E, F with PTB7:$PC_{71}BM$ doped 3% DIO additive as active layer.

Devices	J_{sc} (mA/cm^2)	V_{oc} (V)	FF (%)	PCE (%)
Device A	8.70	0.603	53.6	2.8
Device B	10.48	0.608	54.3	3.5
Device C	10.89	0.609	57.2	3.8
Device D	16.60	0.71	56.0	6.6
Device E	17.56	0.72	58.5	7.5
Device F	17.57	0.73	57.6	7.3

Key: Device A, ITO/ZnO/P3HT:$PC_{61}BM$ (1:1, w/w)/e-MoO_3/Ag; Device B, ITO/ ZnO/PEEMC (4 mg/ml)/P3HT:$PC_{61}BM$ (1:1, w/w)/e-MoO_3/Ag; Device C, ITO/ ZnO/MT-PEEMC (4 mg/ml)/P3HT:$PC_{61}BM$ (1:1, w/w)/e-MoO_3/Ag. Device D, ITO/ ZnO/PTB7:$PC_{71}BM$ (1:1.5, w/w)/e-MoO_3/Ag; Device E, ITO/ZnO/ MT-PEEMC/PTB7:$PC_{71}BM$ (1:1.5, w/w)/e-MoO_3/Ag; Device F, ITO/ZnO/ MT-PEEMC/PTB7:$PC_{71}BM$ (1:1.5, w/w)/s-VO_x/Ag.

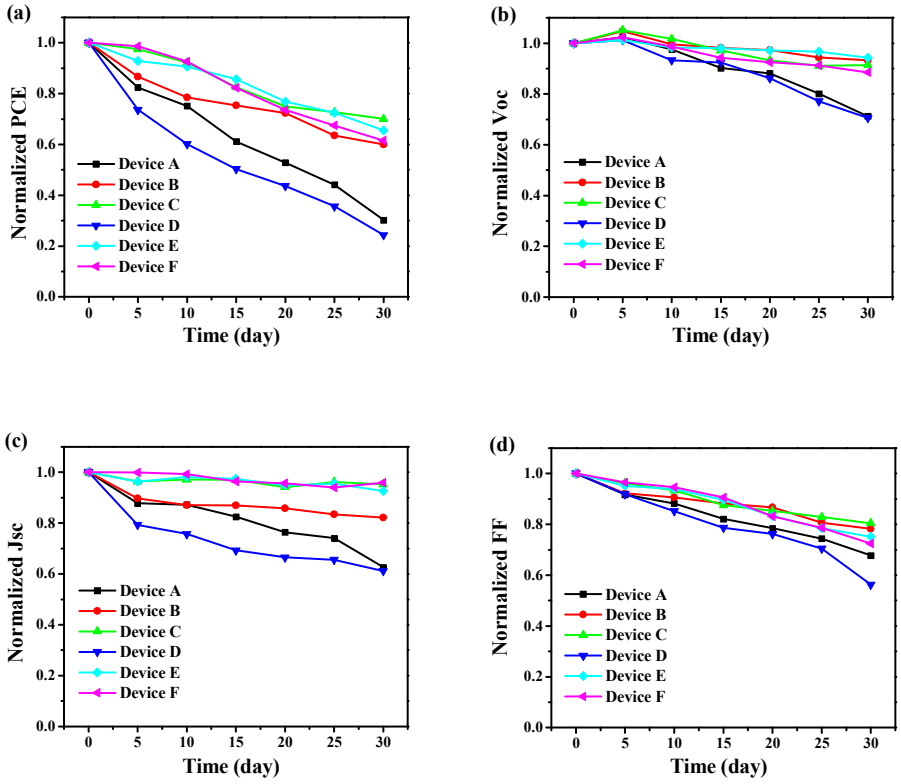

Figure 8. Air-stability test of the unencapsulated structures of Device A-F stored for 30 days under ambient conditions. **(a)** PCE, **(b)** V_{oc}, **(c)** J_{sc}, **(d)** FF.

Highlights

Solution Processed and Self-assembled Polymerizable Fullerenes/Metal Oxide as an Interlayer for High Efficient Inverted Polymer Solar Cells

Lin Hu, Lie Chen, Xiaotian Hu, Yiwang Chen

Self-assembled polymerized fullerenes/ZnO as an efficient interlayer realized a PCE of 7.5% with improved stability in inverted polymer solar cells

Graphical abstract